universe

IMPACT FACTOR 2.5

CITESCORE 4.3

Communication

The Pulsar Timing Array Signal from Infrared Regions of Scalar-Induced Gravitational Waves

Qin Fei

MDPI

https://doi.org/10.3390/universe10060255

universe

MDPI

Communication

The Pulsar Timing Array Signal from Infrared Regions of Scalar-Induced Gravitational Waves

Qin Fei

School of Mathematics and Physics, Hubei Polytechnic University, Huangshi 435003, China; feiqin@hbpu.edu.cn

Abstract: The common-spectrum process, characterized by the Hellings–Downs angular correlation and observed by pulsar timing array collaborations, such as NANOGrav, PPTA, EPTA, and CPTA, can be explained by the scalar-induced gravitational waves (SIGWs). The energy density of SIGWs exhibits universal behavior in the infrared regions. Utilizing a broken power law parameterization for the primordial curvature power spectrum, we clarify the PTA signal through the infrared characteristics of the SIGWs, using Bayesian analysis to provide posterior distributions. Bayesian factors emphasize the statistical preference for the SIGW model over explanations involving supermassive black hole binaries.

Keywords: PTA; scalar-induced gravitational wave; inflation

Citation: Fei, Q. The Pulsar Timing Array Signal from Infrared Regions of Scalar-Induced Gravitational Waves. *Universe* **2024**, *10*, 255. https://doi.org/10.3390/universe10060255

Academic Editor: Nicolas Sanchis-Gual

Received: 22 April 2024
Revised: 1 June 2024
Accepted: 5 June 2024
Published: 7 June 2024

1. Introduction

Linear scalar perturbations, seeded by the primordial curvature perturbations generated during inflation, can construct a second-order perturbation source to induce gravitational waves. These scalar-induced gravitational waves (SIGWs), rich in early Universe information, such as the primordial curvature perturbation at small scales [1,2] and the equation of state of the early Universe [3,4], span a broad frequency range and can be detected by pulsar timing arrays (PTAs) or space-based GW detectors, such as the Laser Interferometer Space Antenna (LISA) [5,6], Taiji [7], or TianQin [8,9]. To induce detectable GWs, the amplitude of the primordial curvature power spectrum should be enhanced by about seven orders of magnitude at small scales compared with large-scale observations, which can be achieved with ultra-slow-roll inflation models [10–34]. Alternatively, accompanied by the SIGWs, the large primordial curvature perturbations can give rise to primordial black holes (PBHs) [1,2,16,35–69] (for the review, see [3,70]), offering explanations for LIGO-Virgo GW events [71,72], dark matter [73–81], and the anomalous orbits of trans-Neptunian objects [82].

Typically, scalar-induced gravitational waves exhibit a peak in the amplitude of the energy density at a specific scale, and this specific scale is denoted as k_p. In the infrared regions $k \ll k_p$, SIGWs resulting from primordial curvature perturbations with a narrow peak follow a universal behavior, specifically

$$\Omega_{\rm GW} \propto \left(f/f_{\rm year}\right)^3 \log_{10}^2(f_p/f), \tag{1}$$

where the term "universal" means that a broad range of models gives the same log-dependent index of the energy density spectrum of SIGWs in the infrared region [54,83–85]. A more effective approach to examining the energy density behavior of SIGWs in the infrared regions involves parameterizing the primordial curvature power spectrum using a broken power law form, $\mathcal{P}_\zeta = A_\zeta (k/k_{p_0})^{n_1}$ for $k < k_{p_0}$ and $\mathcal{P}_\zeta = A_\zeta (k/k_{p_0})^{n_2}$ for $k \geq k_{p_0}$. Within this broken power law framework, a narrow peak in the power spectrum is achieved for sufficiently large absolute values of n_1 and n_2, while a broad peak results for sufficiently small absolute values of these parameters. For the case of a narrow peak with $n_1 > 3/2$, the primordial curvature power spectra generate SIGWs with energy densities in

the infrared regions as in Equation (1), which is independent of n_1 and consistent with the conclusion displayed in Ref. [54,83–85]. For the situation with $n_1 = 3/2$, the energy density in the infrared regions is $\Omega_{\rm GW} \propto \left(f/f_{\rm year}\right)^3 \log_{10}^3(f_p/f)$, exhibiting a slight variation from the situation with a narrower peak, $n_1 > 3/2$. Finally, for the case with $n_1 < 3/2$, the broken power law form yields SIGWs with an exact power-law form in the infrared regions.

Recently, a common-spectrum process, which appears compatible with the Hellings–Downs angular correlation has been announced by PTA collaborations, including the North American Nanohertz Observatory for Gravitational Waves (NANOGrav) [86,87], Parkers Pulsar Timing Array (PPTA) [88,89], European Pulsar Timing Array (EPTA), Indian Pulsar Timing Array (InPTA) [90,91], and Chinese Pulsar Timing Array (CPTA) [92]. Assuming that the signals come from an ensemble of binary supermassive black hole binary (SMBHB) inspirals and the characteristic-strain spectrum is proportional to $f^{-2/3}$, the strain amplitude of the signals is around $2.4^{+0.7}_{-0.6} \times 10^{-15}$ at a reference frequency of 1 yr^{-1} [86]. While supermassive black hole binaries are considered as an explanation [93–99], alternative interpretations include cosmic inflation [94,95], first-order phase transitions [100–107], cosmic strings [108–115], domain walls [116–118], or scalar-induced gravitational waves [4,119–131]. For more about the physical explanation of signals in the PTA band, please refer to the references [132–142]. The feature of the energy density of SIGWs in the infrared regions aligns with the PTA signals, prompting our investigation using the NANOGrav 15-year dataset and EPTA Data Release 2 (DR2).

The organization of this paper is as follows. In Section 2, we give a brief review of the energy density of SIGWs in the infrared regions. The constraint on the SIGWs in the infrared regions from the PTAs data is presented in Section 3, and conclusions are given in Section 4.

2. The Infrared Behavior of SIGWs

In this section, we will give a brief review of the calculation of the energy density of SIGWs and their universal behavior in the infrared regions with the power spectrum of the primordial curvature being chosen as a broken power law form. The metric with perturbations in the Newtonian gauge and cosmological background is [143]

$$\mathrm{d}s^2 = -a^2(\eta)(1+2\Phi)\mathrm{d}\eta^2 + a^2(\eta)\left[(1-2\Phi)\delta_{ij} + \frac{1}{2}h_{ij}\right]\mathrm{d}x^i dx^j, \tag{2}$$

where Φ is the Bardeen potential, a is the scale factor of the Universe, η is the conformal time, and h_{ij} is the tensor perturbation. For the second order of tensor perturbations, the linear order scalar perturbations can construct a second-order source to induce the gravitational waves. The power spectrum of these scalar-induced gravitational waves is [1,2,38,40,144,145]

$$\mathcal{P}_h(k,\eta) = 4\int_0^\infty \mathrm{d}v \int_{|1-v|}^{1+v} \mathrm{d}u \left(\frac{4v^2 - \left(1+v^2-u^2\right)^2}{4vu}\right)^2 \times I^2_{\rm RD}(u,v,x)\mathcal{P}_\zeta(vk)\mathcal{P}_\zeta(uk), \tag{3}$$

where $x = k\eta$, and $\mathcal{P}_\zeta$ is the power spectrum of primordial curvature perturbations generated during inflation. After the horizon re-entry, and at the later time $k\eta \gg 1$, the integrated kernel $I^2_{\rm RD}$ can be expressed as [38]

$$\begin{aligned}\overline{I^2_{\rm RD}(v,u,x\to\infty)} = \frac{1}{2x^2}\left(\frac{3(u^2+v^2-3)}{4u^3v^3}\right)^2 \times \Bigg\{&\pi^2(u^2+v^2-3)^2\Theta\left(v+u-\sqrt{3}\right) \\ &- \left(4uv - (u^2+v^2-3)\log\left|\frac{3-(u+v)^2}{3-(u-v)^2}\right|\right)^2\Bigg\},\end{aligned} \tag{4}$$

where a bar on the top denotes the mean value among several periods. The energy density in gravitational waves is

$$\Omega_{\rm GW}(\eta,k)=\frac{1}{24}\left(\frac{k}{\mathcal{H}(\eta)}\right)^2\overline{\mathcal{P}_h(k,\eta)}. \tag{5}$$

To describe the power spectrum of the primordial curvature perturbations, we use a broken power-law parameterization, which takes the following form

$$\mathcal{P}_\zeta(k)=\begin{cases}A_\zeta\left(\frac{k}{k_{p_0}}\right)^{n_1}, & k\le k_{p_0},\\ A_\zeta\left(\frac{k}{k_{p_0}}\right)^{n_2}, & k>k_{p_0},\end{cases} \tag{6}$$

where k_{p_0} is the peak scale and A_ζ is the amplitude at the peak. To ensure a single peak in the power spectrum at the scale k_{p_0}, the indices of the parameterization (6) should satisfy the condition $n_1>0$ and $n_2<0$. The magnitude of n_1 and n_2 determines the nature of the peak: small absolute values result in a broad peak, while large absolute values produce a narrow peak. Consequently, the broken power-law parameterization is versatile and capable of representing both narrow and broad peak power spectra. By substituting the parameterization (6) into the above equations, we can derive the energy density of scalar-induced gravitational waves in the infrared region,

$$h^2\Omega_{\rm GW}(k)=\begin{cases}A_{GW}\left(\frac{f}{f_{\rm year}}\right)^{2n_1}, & n_1<3/2\\ A_{GW}\left(\frac{f}{f_{\rm year}}\right)^{3}\log_{10}^3(f_p/f), & n_1=3/2,\\ A_{GW}\left(\frac{f}{f_{\rm year}}\right)^{3}\log_{10}^2(f_p/f), & n_1>3/2,\end{cases} \tag{7}$$

where the relation of the wave number k and the frequency f is

$$f=\frac{k}{2\pi}\simeq 1.6\,{\rm nHz}\left(\frac{k}{10^6\ {\rm Mpc}^{-1}}\right), \tag{8}$$

and $f_{\rm year}$ represents the frequency corresponding to one year. For the scenario of a narrow peak with $n_1>3/2$, the behavior of the energy density of SIGWs in the infrared regions is independent of the model n_1 and consistent with the conclusion in Ref. [54,83–85]. In contrast, for the broad peak with $n_1<3/2$, the behavior of the energy density of SIGWs in the infrared regions follows an exact power law form.

3. Results

The increasing feature of the energy density of SIGWs in infrared regions aligns with the recent PTA signals. To explain the PTA signal and obtain the constraints on the SIGWs described by Equation (7), we independently perform a Bayesian analysis on the NANOGrav 15-year dataset and the EPTA DR2, respectively. In the Bayesian analysis, we employ the `Bilby` gravitational wave inference library [146] using nested sampling with the `dynesty` algorithm [147]. The NANOGrav dataset consists of 14 frequency bins from the NANOGrav 15-year dataset [86,94] and the EPTA dataset consists of 9 bins from the EPTA DR2 [91,95]. To compute the log-likelihood, we first calculate the SIGW energy density at all the frequency bins for each dataset. We then evaluate the log probabilities from independent kernel density estimates of the energy density at each bin. Finally, we obtain the log-likelihood by taking the sum of all these log probability terms for each dataset [148]. Consequently, the likelihood can be expressed as

$$\ln\mathcal{L}_\mathcal{D}(\mathbf{\Theta})=\sum_{i=1}^{n_\mathcal{D}}\ln\mathcal{L}_i(\Omega_{\rm GW}(f_i,\mathbf{\Theta})), \tag{9}$$

where $\mathbf{\Theta} = \{\mathcal{A}_{\rm GW},\ n_1,\ f_p\}$ is the collection of parameters presented in Equation (7), f_i is the frequency of each bin, the label $\mathcal{D} = \{\text{nano}, \text{epta}\}$ denotes the NANOGrav dataset and EPTA dataset, and $\{n_{\rm nano} = 14,\ n_{\rm epta} = 9\}$. The natural logarithm of the Bayes factors is defined as

$$\ln \mathcal{B}_{10}(\mathcal{D}) = \ln\left(\frac{p(\mathcal{D}|\mathcal{M}_1)}{p(\mathcal{D}|\mathcal{M}_0)}\right), \tag{10}$$

where $p(\mathcal{D}|\mathcal{M})$ is the model evidence. In this work, we choose the fiducial model $\mathcal{M}_0$ as the SMBHB model, and the model $\mathcal{M}_1$ is given by Equation (7).

In Table 1, we display the priors of the parameters $\{\mathcal{A}_{\rm GW},\ n_1,\ f_p\}$. The priors of the parameters are uniform or log-uniform distributions.

Table 1. The priors, maximum posterior values, 1-σ credible interval bounds of posteriors, and Bayes factor for the model are described by Equation (7). The labels "nano" and "epta" denote the Bayesian analysis conducted using the NANOGrav 15-year dataset and EPTA DR2, respectively. The fiducial model $\mathcal{M}_0$ is SMBHB model. The symbol $\mathcal{U}$ denotes the uniform distribution.

Model	Parameters	Prior	Posterior (Nano)	Posterior (Epta)	ln $\mathcal{B}$ (Nano)	ln $\mathcal{B}$ (Epta)
$n_1 < 3/2$	$\log_{10}A_{\rm GW}$	$U[-10,-5]$	$-7.17^{+0.24}_{-0.25}$	$-7.06^{+0.23}_{-0.32}$	4.4	4.8
	n_1	$U[0,1.5]$	$+0.95^{+0.16}_{-0.17}$	$+1.17^{+0.19}_{-0.24}$		
$n_1 = 3/2$	$\log_{10}A_{\rm GW}$	$U[-10,-5]$	$-8.02^{+0.42}_{-0.68}$	$-9.27^{+0.68}_{-0.43}$	4.5	5.3
	$\log_{10}(f_p/\text{Hz})$	$U[-9,-3]$	$-6.67^{+0.96}_{-0.37}$	$-4.94^{+1.27}_{-1.25}$		
$n_1 > 3/2$	$\log_{10}A_{\rm GW}$	$U[-10,-5]$	$-7.20^{+0.31}_{-0.53}$	$-8.31^{+0.54}_{-0.40}$	4.0	5.2
	$\log_{10}(f_p/\text{Hz})$	$U[-9,-3]$	$-7.09^{+0.80}_{-0.26}$	$-5.20^{+1.49}_{-1.31}$		
SMBHB	$\log_{10}A_{\rm GW}$	$U[-10,-5]$	$-8.14^{+0.13}_{-0.16}$	$-8.21^{+0.18}_{-0.08}$	–	–

The posteriors for the parameters are shown in Figures 1–3, where the left panel and right panel use the NANOGrav 15-year dataset and EPTA DR2, respectively. For the priors listed in Table 1, increasing the interval of the bounds results in almost the same posterior, with the Bayes factor changing slowly as the interval becomes larger. Therefore, priors with larger interval bounds do not significantly affect the posterior and the final conclusions. The corresponding maximum posterior values, 1-σ credible interval bounds, and Bayes factors are presented in Table 1, where the labels "nano" and "epta" denote the result by using the NANOGrav dataset and EPTA DR2, respectively. For the broad peak with $n_1 < 3/2$, the energy density of SIGWs obeys the power law form, and the posterior, displayed in Figure 1, is consistent with the results given in the NANOGrav collaboration [94]. By using the NANOGrav 15-year dataset, the maximum posterior values and 1-σ credible interval bounds of posteriors are $n_1 = 0.95^{+0.16}_{-0.17}$ and $\log_{10} A_{\rm GW} = -7.17^{+0.24}_{-0.25}$; by using the EPTA DR2; they are $n_1 = 1.17^{+0.19}_{-0.24}$ and $\log_{10} A_{\rm GW} = -7.06^{+0.23}_{-0.32}$. For the intermediate case with $n_1 = 3/2$, the posterior of the parameters is illustrated in Figure 2. By using the NANOGrav 15-year dataset, the maximum posterior values and 1-σ credible interval bounds of posteriors are $\log_{10} f_p/\text{Hz} = -6.67^{+0.96}_{-0.37}$ and $\log_{10} A_{\rm GW} = -8.02^{+0.42}_{-0.68}$, and by using the EPTA DR2, they are $\log_{10} f_p/\text{Hz} = -4.94^{+1.27}_{-1.25}$ and $\log_{10} A_{\rm GW} = -9.27^{+0.68}_{-0.43}$. For the narrow peak with $n_1 > 3/2$, the energy density of SIGWs in infrared regions has a universal log-dependent form, which is independent of the index n_1. The posterior for the parameters is shown in Figure 3; by using the NANOGrav 15-year dataset, we have $\log_{10} f_p/\text{Hz} = -7.09^{+0.80}_{-0.26}$ and $\log_{10} A_{\rm GW} = -7.20^{+0.31}_{-0.53}$; and by using the EPTA DR2, we have $\log_{10} f_p/\text{Hz} = -5.20^{+1.49}_{-1.31}$ and $\log_{10} A_{\rm GW} = -8.31^{+0.54}_{-0.40}$.

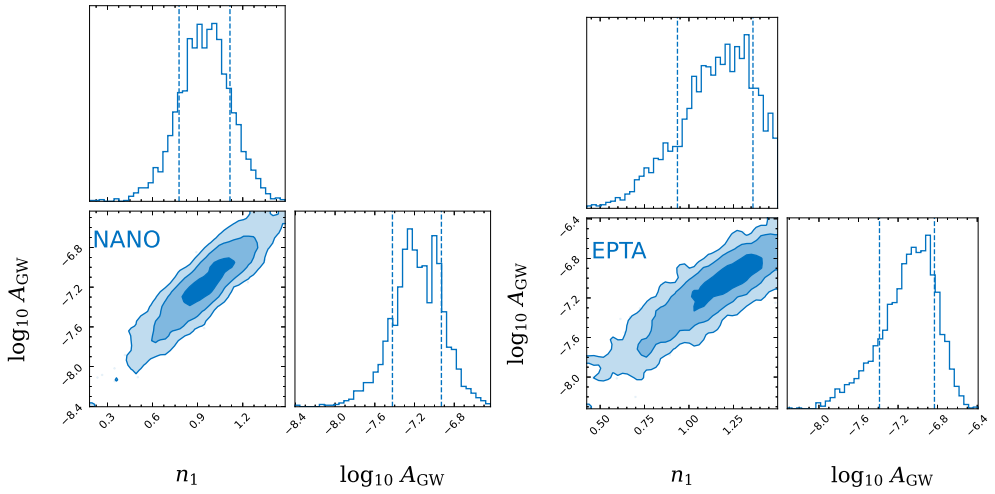

Figure 1. The posterior of the parameters for the broad peak case with $n_1 < 3/2$, and the blue regions denote 1 σ, 2 σ, and 3 σ confidence regions. The left and right panels use the NANOGrav 15-year dataset and EPTA DR2, respectively. The dashed vertical blue lines denote 0.16 and 0.84 qualities, respectively.

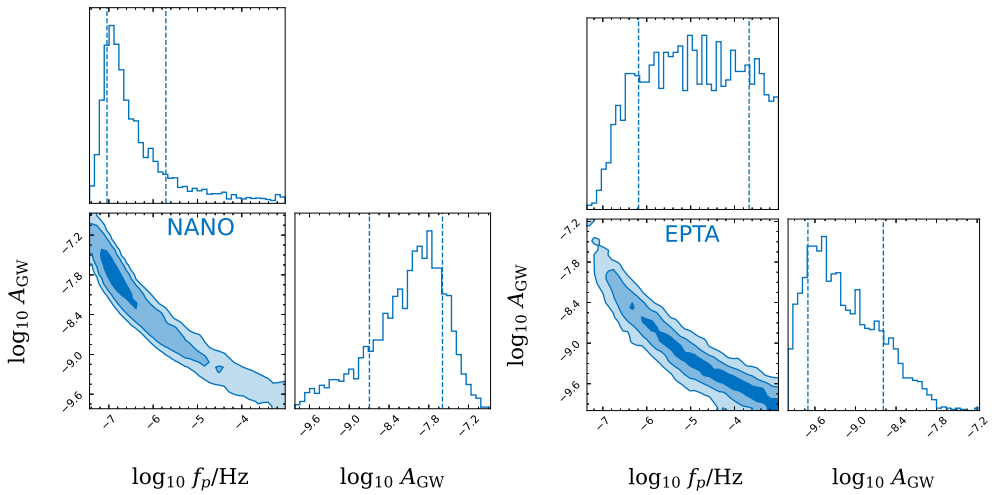

Figure 2. The posterior of the parameters for the intermediate case with $n_1 = 3/2$, and the blue regions denote 1 σ, 2 σ, and 3 σ confidence regions.

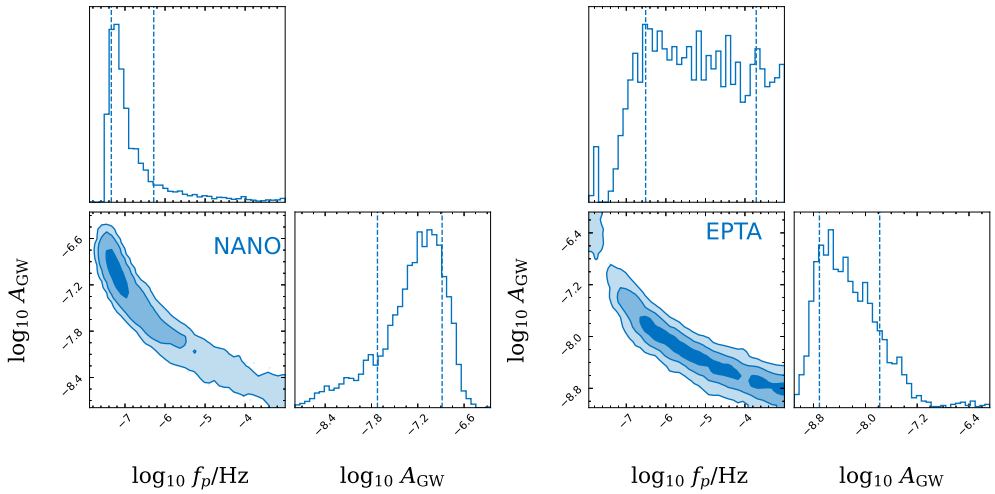

Figure 3. The posterior of the parameters for the narrow peak case with $n_1 > 3/2$, and the blue regions denote 1 σ, 2 σ, and 3 σ confidence regions.

Utilizing the maximum posterior values from Table 1, and taking them into Equation (7), we visualize the energy density of the SIGWs in the infrared regions in Figure 4. The left panel and right panel are the fittings of the NANOGrav 15-year dataset and EPTA DR2, respectively. The blue and gray violins represent the observational bins from the NANOGrav 15-year dataset and EPTA DR2 dataset. Meanwhile, the black, green, and red curves correspond to the energy density of SIGWs from broad ($n_1 < 3/2$), intermediate ($n_1 = 3/2$), and narrow peaks ($n_1 > 3/2$), respectively. The three energy density curves are closely packed both for the NANOGrav dataset and EPTA dataset, making it challenging to distinguish between the three models. This result is also supported by the natural logarithm of the Bayes factors listed in Table 1.

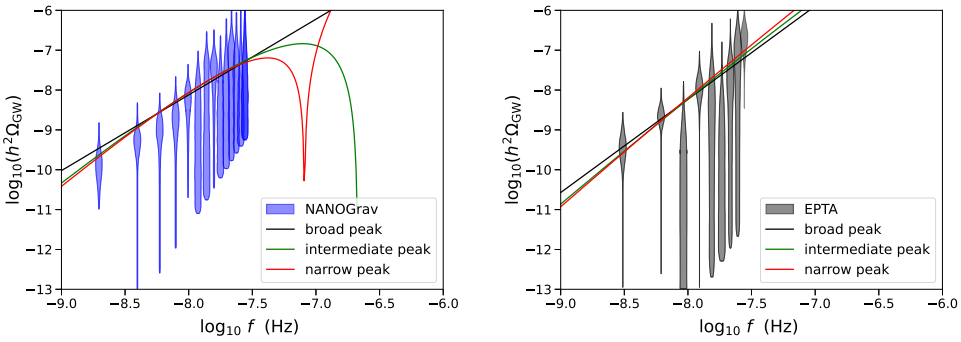

Figure 4. The energy density of the SIGWs given by Equation (7). The broad, intermediate, and narrow peaks denote the case with $n_1 < 3/2$, $n_1 = 3/2$, and $n_1 > 3/2$, respectively. The blue violins in the left panel and the gray violins in the right panel are the constraints from the NANOGrav 15-year dataset and EPTA DR2, respectively.

4. Discussion and Conclusions

The common-spectrum process, characterized by the Hellings–Downs angular correlation detected by NANOGrav, PPTA, EPTA, and CPTA collaborations can be accounted for by scalar-induced gravitational waves. The energy density of SIGWs arising from the primordial curvature power spectrum with a narrow peak has a universal log-dependent form in the infrared regions. An effective parameterization of the primordial curvature power spectrum is the broken power law form, given by $\mathcal{P}_\zeta = A_\zeta (k/k_{p_0})^{n_1}$ for $k < k_{p_0}$ and $\mathcal{P}_\zeta = A_\zeta (k/k_{p_0})^{n_2}$ for $k \geq k_{p_0}$. For $n_1 > 3/2$, this form gives a power spectrum with a narrow peak, and the corresponding SIGWs exhibit the universal form $h^2\Omega_{\rm GW} = A_{GW} \left(f/f_{\rm year}\right)^3 \log_{10}^2(f_p/f)$; for $n_1 = 3/2$, this intermediate case induces $h^2\Omega_{\rm GW} = A_{GW} \left(f/f_{\rm year}\right)^3 \log_{10}^3(f_p/f)$; and for $n_1 < 3/2$, the primordial curvature power spectrum with a broad peak produces SIGWs with an energy density in the infrared regions exhibiting an exact power-law form.

Utilizing Bayesian analysis on the dataset of NANOGrav 15-year data and EPTA DR2 independently, we determine the posterior distribution of parameters in the SIGW energy density in Equation (7). For the scenario where the primordial curvature power spectrum features a broad peak with $n_1 < 3/2$, the maximum posterior values and 1-σ credible interval bounds of posteriors by using NANOGrav dataset are $n_1 = 0.95^{+0.16}_{-0.17}$ and $\log_{10} A_{\rm GW} = -7.17^{+0.24}_{-0.25}$, and they are $n_1 = 1.17^{+0.19}_{-0.24}$ and $\log_{10} A_{\rm GW} = -7.06^{+0.23}_{-0.32}$ by using EPTA DR2. For the intermediate case with $n_1 = 3/2$, we have $\log_{10} f_p/{\rm Hz} = -6.67^{+0.96}_{-0.37}$ and $\log_{10} A_{\rm GW} = -8.02^{+0.42}_{-0.68}$ by using NANOGrav dataset, and $\log_{10} f_p/{\rm Hz} = -4.94^{+1.27}_{-1.25}$ and $\log_{10} A_{\rm GW} = -9.27^{+0.68}_{-0.43}$ by using EPTA DR2. In the case that the primordial curvature power spectrum has a narrow peak with $n_1 > 3/2$, we obtain $\log_{10} f_p/{\rm Hz} = -7.09^{+0.80}_{-0.26}$ and $\log_{10} A_{\rm GW} = -7.20^{+0.31}_{-0.53}$ by using the NANOGrav dataset, and $\log_{10} f_p/{\rm Hz} = -5.20^{+1.49}_{-1.31}$ and $\log_{10} A_{\rm GW} = -8.31^{+0.54}_{-0.40}$ by using the EPTA DR2. Compared to interpreting the signal as a stochastic background from supermassive black hole binaries, the natural logarithm of the Bayes factors for these three models are around $\ln \mathcal{B} \approx 4$ by using the NANOGrav

dataset, and $\ln \mathcal{B} \approx 5$ by using the EPTA DR2. Consequently, the PTA signal favors the SIGW explanation over SMBHBs, yet cannot distinguish between broad and narrow peak scenarios. Besides SIGWs, other cosmological processes, such as domain walls and phase transitions, are also favored by the PTA dataset in terms of Bayesian analysis. To confirm the source of this PTA signal, we require information from other frequency bands. Future space-based gravitational wave detectors, such as LISA, TianQin, and Taiji, may have the opportunity to provide that information.

Funding: This research was supported in part by the National Natural Science Foundation of China under Grant No. 12305060 and the Talent-Introduction Program of Hubei Polytechnic University under Grant No.19xjk25R.

Data Availability Statement: Data are contained within the article.

Conflicts of Interest: The author declares no conflicts of interest.

References

1. Ananda, K.N.; Clarkson, C.; Wands, D. The Cosmological gravitational wave background from primordial density perturbations. *Phys. Rev. D* **2007**, *75*, 123518. [CrossRef]
2. Baumann, D.; Steinhardt, P.J.; Takahashi, K.; Ichiki, K. Gravitational Wave Spectrum Induced by Primordial Scalar Perturbations. *Phys. Rev. D* **2007**, *76*, 084019. [CrossRef]
3. Domènech, G. Scalar Induced Gravitational Waves Review. *Universe* **2021**, *7*, 398. [CrossRef]
4. Liu, L.; Chen, Z.C.; Huang, Q.G. Probing the equation of state of the early Universe with pulsar timing arrays. *J. Cosmol. Astropart. Phys.* **2023**, *11*, 071. [CrossRef]
5. Danzmann, K. LISA: An ESA cornerstone mission for a gravitational wave observatory. *Class. Quant. Grav.* **1997**, *14*, 1399–1404. [CrossRef]
6. Amaro-Seoane, P.; Audley, H.; Babak, S.; Baker, J.; Barausse, E.; Bender, P.; Berti, E.; Binetruy, P.; Born, M.; Bortoluzzi, D.; et al. Laser Interferometer Space Antenna. *arXiv* **2017**, arXiv:1702.00786.
7. Hu, W.R.; Wu, Y.L. The Taiji Program in Space for gravitational wave physics and the nature of gravity. *Natl. Sci. Rev.* **2017**, *4*, 685–686. [CrossRef]
8. Luo, J.; Chen, L.; Duan, H.; Gong, Y.; Hu, S.; Ji, J.; Liu, Q.; Mei, J.; Milyukov, V.; Sazhin, M.; et al. TianQin: A space-borne gravitational wave detector. *Class. Quant. Grav.* **2016**, *33*, 035010. [CrossRef]
9. Gong, Y.; Luo, J.; Wang, B. Concepts and status of Chinese space gravitational wave detection projects. *Nat. Astron.* **2021**, *5*, 881–889. [CrossRef]
10. Martin, J.; Motohashi, H.; Suyama, T. Ultra Slow-Roll Inflation and the non-Gaussianity Consistency Relation. *Phys. Rev. D* **2013**, *87*, 023514. [CrossRef]
11. Motohashi, H.; Starobinsky, A.A.; Yokoyama, J. Inflation with a constant rate of roll. *J. Cosmol. Astropart. Phys.* **2015**, *09*, 018. [CrossRef]
12. Yi, Z.; Gong, Y. On the constant-roll inflation. *J. Cosmol. Astropart. Phys.* **2018**, *03*, 052. [CrossRef]
13. Germani, C.; Prokopec, T. On primordial black holes from an inflection point. *Phys. Dark Univ.* **2017**, *18*, 6–10. [CrossRef]
14. Motohashi, H.; Hu, W. Primordial Black Holes and Slow-Roll Violation. *Phys. Rev. D* **2017**, *96*, 063503. [CrossRef]
15. Ezquiaga, J.M.; Garcia-Bellido, J.; Ruiz Morales, E. Primordial Black Hole production in Critical Higgs Inflation. *Phys. Lett. B* **2018**, *776*, 345–349. [CrossRef]
16. Di, H.; Gong, Y. Primordial black holes and second order gravitational waves from ultra-slow-roll inflation . *J. Cosmol. Astropart. Phys.* **2018**, *07*, 007. [CrossRef]
17. Gao, Q.; Gong, Y.; Yi, Z. On the constant-roll inflation with large and small η_H. *Universe* **2019**, *5*, 215. [CrossRef]
18. Lin, J.; Gao, Q.; Gong, Y.; Lu, Y.; Zhang, C.; Zhang, F. Primordial black holes and secondary gravitational waves from k and G inflation. *Phys. Rev. D* **2020**, *101*, 103515. [CrossRef]
19. Lin, J.; Gao, S.; Gong, Y.; Lu, Y.; Wang, Z.; Zhang, F. Primordial black holes and scalar induced gravitational waves from Higgs inflation with noncanonical kinetic term. *Phys. Rev. D* **2023**, *107*, 043517. [CrossRef]
20. Gao, Q.; Gong, Y.; Yi, Z. Primordial black holes and secondary gravitational waves from natural inflation. *Nucl. Phys. B* **2021**, *969*, 115480. [CrossRef]
21. Gao, Q. Primordial black holes and secondary gravitational waves from chaotic inflation. *Sci. China Phys. Mech. Astron.* **2021**, *64*, 280411. [CrossRef]
22. Yi, Z.; Gong, Y.; Wang, B.; Zhu, Z.h. Primordial black holes and secondary gravitational waves from the Higgs field. *Phys. Rev. D* **2021**, *103*, 063535. [CrossRef]
23. Yi, Z.; Gao, Q.; Gong, Y.; Zhu, Z.h. Primordial black holes and scalar-induced secondary gravitational waves from inflationary models with a noncanonical kinetic term. *Phys. Rev. D* **2021**, *103*, 063534. [CrossRef]
24. Yi, Z.; Zhu, Z.H. NANOGrav signal and LIGO-Virgo primordial black holes from the Higgs field. *J. Cosmol. Astropart. Phys.* **2022**, *05*, 046. [CrossRef]

25. Yi, Z. Primordial black holes and scalar-induced gravitational waves from the generalized Brans-Dicke theory. *J. Cosmol. Astropart. Phys.* **2023**, *03*, 048. [CrossRef]
26. Zhang, F.; Gong, Y.; Lin, J.; Lu, Y.; Yi, Z. Primordial non-Gaussianity from G-inflation. *J. Cosmol. Astropart. Phys.* **2021**, *04*, 045. [CrossRef]
27. Pi, S.; Zhang, Y.l.; Huang, Q.G.; Sasaki, M. Scalaron from R^2-gravity as a heavy field. *J. Cosmol. Astropart. Phys.* **2018**, *05*, 042. [CrossRef]
28. Kamenshchik, A.Y.; Tronconi, A.; Vardanyan, T.; Venturi, G. Non-Canonical Inflation and Primordial Black Holes Production. *Phys. Lett. B* **2019**, *791*, 201–205. [CrossRef]
29. Fu, C.; Wu, P.; Yu, H. Primordial Black Holes from Inflation with Nonminimal Derivative Coupling. *Phys. Rev. D* **2019**, *100*, 063532. [CrossRef]
30. Fu, C.; Wu, P.; Yu, H. Scalar induced gravitational waves in inflation with gravitationally enhanced friction. *Phys. Rev. D* **2020**, *101*, 023529. [CrossRef]
31. Zhang, F. Primordial black holes and scalar induced gravitational waves from the E model with a Gauss-Bonnet term. *Phys. Rev. D* **2022**, *105*, 063539. [CrossRef]
32. Cai, R.G.; Chen, C.; Fu, C. Primordial black holes and stochastic gravitational wave background from inflation with a noncanonical spectator field. *Phys. Rev. D* **2021**, *104*, 083537. [CrossRef]
33. Chen, P.; Koh, S.; Tumurtushaa, G. Primordial black holes and induced gravitational waves from inflation in the Horndeski theory of gravity. *arXiv* **2021**, arXiv:2107.08638.
34. Karam, A.; Koivunen, N.; Tomberg, E.; Vaskonen, V.; Veermäe, H. Anatomy of single-field inflationary models for primordial black holes. *J. Cosmol. Astropart. Phys.* **2023**, *03*, 013. [CrossRef]
35. Hawking, S. Gravitationally collapsed objects of very low mass. *Mon. Not. Roy. Astron. Soc.* **1971**, *152*, 75. [CrossRef]
36. Carr, B.J.; Hawking, S.W. Black holes in the early Universe. *Mon. Not. Roy. Astron. Soc.* **1974**, *168*, 399–415. [CrossRef]
37. Saito, R.; Yokoyama, J. Gravitational wave background as a probe of the primordial black hole abundance. *Phys. Rev. Lett.* **2009**, *102*, 161101; Erratum in *Phys. Rev. Lett.* **2011**, *107*, 069901. [CrossRef] [PubMed]
38. Kohri, K.; Terada, T. Semianalytic calculation of gravitational wave spectrum nonlinearly induced from primordial curvature perturbations. *Phys. Rev. D* **2018**, *97*, 123532. [CrossRef]
39. Cheng, S.L.; Lee, W.; Ng, K.W. Primordial black holes and associated gravitational waves in axion monodromy inflation. *J. Cosmol. Astropart. Phys.* **2018**, *07*, 001. [CrossRef]
40. Lu, Y.; Gong, Y.; Yi, Z.; Zhang, F. Constraints on primordial curvature perturbations from primordial black hole dark matter and secondary gravitational waves. *J. Cosmol. Astropart. Phys.* **2019**, *12*, 031. [CrossRef]
41. Cai, R.G.; Pi, S.; Wang, S.J.; Yang, X.Y. Resonant multiple peaks in the induced gravitational waves. *J. Cosmol. Astropart. Phys.* **2019**, *05*, 013. [CrossRef]
42. Cai, R.g.; Pi, S.; Sasaki, M. Gravitational Waves Induced by non-Gaussian Scalar Perturbations. *Phys. Rev. Lett.* **2019**, *122*, 201101. [CrossRef] [PubMed]
43. Cai, R.G.; Pi, S.; Wang, S.J.; Yang, X.Y. Pulsar Timing Array Constraints on the Induced Gravitational Waves. *J. Cosmol. Astropart. Phys.* **2019**, *10*, 059. [CrossRef]
44. Cai, R.G.; Guo, Z.K.; Liu, J.; Liu, L.; Yang, X.Y. Primordial black holes and gravitational waves from parametric amplification of curvature perturbations. *J. Cosmol. Astropart. Phys.* **2020**, *06*, 013. [CrossRef]
45. Wu, Y. Merger history of primordial black-hole binaries. *Phys. Rev. D* **2020**, *101*, 083008. [CrossRef]
46. Domènech, G.; Pi, S.; Sasaki, M. Induced gravitational waves as a probe of thermal history of the universe. *J. Cosmol. Astropart. Phys.* **2020**, *08*, 017. [CrossRef]
47. Liu, L.; Guo, Z.K.; Cai, R.G. Effects of the surrounding primordial black holes on the merger rate of primordial black hole binaries. *Phys. Rev. D* **2019**, *99*, 063523. [CrossRef]
48. Liu, L.; Guo, Z.K.; Cai, R.G. Effects of the merger history on the merger rate density of primordial black hole binaries. *Eur. Phys. J. C* **2019**, *79*, 717. [CrossRef]
49. Liu, L.; Guo, Z.K.; Cai, R.G.; Kim, S.P. Merger rate distribution of primordial black hole binaries with electric charges. *Phys. Rev. D* **2020**, *102*, 043508. [CrossRef]
50. Liu, L.; Yang, X.Y.; Guo, Z.K.; Cai, R.G. Testing primordial black hole and measuring the Hubble constant with multiband gravitational-wave observations. *J. Cosmol. Astropart. Phys.* **2023**, *01*, 006. [CrossRef]
51. Liu, L.; You, Z.Q.; Wu, Y.; Chen, Z.C. Constraining the merger history of primordial-black-hole binaries from GWTC-3. *Phys. Rev. D* **2023**, *107*, 063035. [CrossRef]
52. Chen, Z.C.; Yuan, C.; Huang, Q.G. Pulsar Timing Array Constraints on Primordial Black Holes with NANOGrav 11-Year Dataset. *Phys. Rev. Lett.* **2020**, *124*, 251101. [CrossRef] [PubMed]
53. Yuan, C.; Chen, Z.C.; Huang, Q.G. Scalar induced gravitational waves in different gauges. *Phys. Rev. D* **2020**, *101*, 063018. [CrossRef]
54. Yuan, C.; Chen, Z.C.; Huang, Q.G. Log-dependent slope of scalar induced gravitational waves in the infrared regions. *Phys. Rev. D* **2020**, *101*, 043019. [CrossRef]
55. Yuan, C.; Chen, Z.C.; Huang, Q.G. Probing primordial–black-hole dark matter with scalar induced gravitational waves. *Phys. Rev. D* **2019**, *100*, 081301. [CrossRef]

56. Carr, B.; Kohri, K.; Sendouda, Y.; Yokoyama, J. Constraints on primordial black holes. *Rept. Prog. Phys.* **2021**, *84*, 116902. [CrossRef] [PubMed]
57. Liu, L.; Christiansen, O.; Guo, Z.K.; Cai, R.G.; Kim, S.P. Gravitational and electromagnetic radiation from binary black holes with electric and magnetic charges: Circular orbits on a cone. *Phys. Rev. D* **2020**, *102*, 103520. [CrossRef]
58. Liu, L.; Christiansen, O.; Ruan, W.H.; Guo, Z.K.; Cai, R.G.; Kim, S.P. Gravitational and electromagnetic radiation from binary black holes with electric and magnetic charges: Elliptical orbits on a cone. *Eur. Phys. J. C* **2021**, *81*, 1048. [CrossRef]
59. Yi, Z.; Fei, Q. Constraints on primordial curvature spectrum from primordial black holes and scalar-induced gravitational waves. *Eur. Phys. J. C* **2023**, *83*, 82. [CrossRef]
60. Liu, L.; Kim, S.P. Gravitational and electromagnetic radiations from binary black holes with electric and magnetic charges. In Proceedings of the 17th Italian-Korean Symposium on Relativistic Astrophysics, Gunsan-si, Republic of Korea, 2–6 August 2021.
61. Chen, Z.C.; Huang, Q.G. Merger Rate Distribution of Primordial-Black-Hole Binaries. *Astrophys. J.* **2018**, *864*, 61. [CrossRef]
62. Chen, Z.C.; Huang, F.; Huang, Q.G. Stochastic Gravitational-wave Background from Binary Black Holes and Binary Neutron Stars and Implications for LISA. *Astrophys. J.* **2019**, *871*, 97. [CrossRef]
63. Chen, Z.C.; Huang, Q.G. Distinguishing Primordial Black Holes from Astrophysical Black Holes by Einstein Telescope and Cosmic Explorer. *J. Cosmol. Astropart. Phys.* **2020**, *08*, 039. [CrossRef]
64. Chen, Z.C.; Yuan, C.; Huang, Q.G. Confronting the primordial black hole scenario with the gravitational-wave events detected by LIGO-Virgo. *Phys. Lett. B* **2022**, *829*, 137040. [CrossRef]
65. Chen, Z.C.; Du, S.S.; Huang, Q.G.; You, Z.Q. Constraints on primordial-black-hole population and cosmic expansion history from GWTC-3. *J. Cosmol. Astropart. Phys.* **2023**, *03*, 024. [CrossRef]
66. Liu, L.; Kim, S.P. Merger rate of charged black holes from the two-body dynamical capture. *J. Cosmol. Astropart. Phys.* **2022**, *03*, 059. [CrossRef]
67. Zheng, L.M.; Li, Z.; Chen, Z.C.; Zhou, H.; Zhu, Z.H. Towards a reliable reconstruction of the power spectrum of primordial curvature perturbation on small scales from GWTC-3. *Phys. Lett. B* **2023**, *838*, 137720. [CrossRef]
68. Chen, Z.C.; Kim, S.P.; Liu, L. Gravitational and electromagnetic radiation from binary black holes with electric and magnetic charges: Hyperbolic orbits on a cone. *Commun. Theor. Phys.* **2023**, *75*, 065401. [CrossRef]
69. Meng, D.S.; Yuan, C.; Huang, Q.G. Primordial black holes generated by the non-minimal spectator field. *Sci. China Phys. Mech. Astron.* **2023**, *66*, 280411. [CrossRef]
70. Sasaki, M.; Suyama, T.; Tanaka, T.; Yokoyama, S. Primordial black holes—Perspectives in gravitational wave astronomy. *Class. Quant. Grav.* **2018**, *35*, 063001. [CrossRef]
71. Bird, S.; Cholis, I.; Muñoz, J.B.; Ali-Haïmoud, Y.; Kamionkowski, M.; Kovetz, E.D.; Raccanelli, A.; Riess, A.G. Did LIGO detect dark matter? *Phys. Rev. Lett.* **2016**, *116*, 201301. [CrossRef] [PubMed]
72. Sasaki, M.; Suyama, T.; Tanaka, T.; Yokoyama, S. Primordial Black Hole Scenario for the Gravitational-Wave Event GW150914. *Phys. Rev. Lett.* **2016**, *117*, 061101; Erratum in *Phys. Rev. Lett.* **2018**, *121*, 059901. [CrossRef] [PubMed]
73. Ivanov, P.; Naselsky, P.; Novikov, I. Inflation and primordial black holes as dark matter. *Phys. Rev. D* **1994**, *50*, 7173–7178. [CrossRef] [PubMed]
74. Frampton, P.H.; Kawasaki, M.; Takahashi, F.; Yanagida, T.T. Primordial Black Holes as All Dark Matter. *J. Cosmol. Astropart. Phys* **2010**, *04*, 023. [CrossRef]
75. Belotsky, K.M.; Dmitriev, A.D.; Esipova, E.A.; Gani, V.A.; Grobov, A.V.; Khlopov, M.Y.; Kirillov, A.A.; Rubin, S.G.; Svadkovsky, I.V. Signatures of primordial black hole dark matter. *Mod. Phys. Lett. A* **2014**, *29*, 1440005. [CrossRef]
76. Khlopov, M.Y.; Rubin, S.G.; Sakharov, A.S. Primordial structure of massive black hole clusters. *Astropart. Phys.* **2005**, *23*, 265. [CrossRef]
77. Carr, B.; Kuhnel, F.; Sandstad, M. Primordial Black Holes as Dark Matter. *Phys. Rev. D* **2016**, *94*, 083504. [CrossRef]
78. Inomata, K.; Kawasaki, M.; Mukaida, K.; Tada, Y.; Yanagida, T.T. Inflationary Primordial Black Holes as All Dark Matter. *Phys. Rev. D* **2017**, *96*, 043504. [CrossRef]
79. García-Bellido, J. Massive Primordial Black Holes as Dark Matter and their detection with Gravitational Waves. *J. Phys. Conf. Ser.* **2017**, *840*, 012032. [CrossRef]
80. Kovetz, E.D. Probing Primordial-Black-Hole Dark Matter with Gravitational Waves. *Phys. Rev. Lett.* **2017**, *119*, 131301. [CrossRef] [PubMed]
81. Carr, B.; Kuhnel, F. Primordial Black Holes as Dark Matter: Recent Developments. *Ann. Rev. Nucl. Part. Sci.* **2020**, *70*, 355–394. [CrossRef]
82. Scholtz, J.; Unwin, J. What if Planet 9 is a Primordial Black Hole? *Phys. Rev. Lett.* **2020**, *125*, 051103. [CrossRef] [PubMed]
83. Cai, R.G.; Pi, S.; Sasaki, M. Universal infrared scaling of gravitational wave background spectra. *Phys. Rev. D* **2020**, *102*, 083528. [CrossRef]
84. Xu, W.T.; Liu, J.; Gao, T.J.; Guo, Z.K. Gravitational waves from double-inflection-point inflation. *Phys. Rev. D* **2020**, *101*, 023505. [CrossRef]
85. Pi, S.; Sasaki, M. Gravitational Waves Induced by Scalar Perturbations with a Lognormal Peak. *J. Cosmol. Astropart. Phys.* **2020**, *09*, 037. [CrossRef]

86. Agazie, G.; Anumarlapudi, A.; Archibald, A.M.; Arzoumanian, Z.; Baker, P.T.; Bécsy, B.; Blecha, L.; Brazier, A.; Brook, P.R.; Burke-Spolaor, S.; et al. The NANOGrav 15 yr Data Set: Evidence for a Gravitational-wave Background. *Astrophys. J. Lett.* **2023**, *951*, L8. [CrossRef]
87. Agazie, G.; Anumarlapudi, A.; Archibald, A.M.; Arzoumanian, Z.; Baker, P.T.; Bécsy, B.; Blecha, L.; Brazier, A.; Brook, P.R.; Burke-Spolaor, S.; et al. The NANOGrav 15 yr Data Set: Observations and Timing of 68 Millisecond Pulsars. *Astrophys. J. Lett.* **2023**, *951*, L9. [CrossRef]
88. Zic, A.; Reardon, D.J.; Kapur, A.; Hobbs, G.; Mandow, R.; Curyło, M.; Shannon, R.M.; Askew, J.; Bailes, M.; Bhat, N.D.R.; et al. The Parkes Pulsar Timing Array third data release. *Publ. Astron. Soc. Austral.* **2023**, *40*, e049. [CrossRef]
89. Reardon, D.J.; Zic, A.; Shannon, R.M.; Hobbs, G.B.; Bailes, M.; Marco, V.D.; Kapur, A.; Rogers, A.F.; Thrane, E.; Askew, J.; et al. Search for an Isotropic Gravitational-wave Background with the Parkes Pulsar Timing Array. *Astrophys. J. Lett.* **2023**, *951*, L6. [CrossRef]
90. Antoniadis, J.; Babak, S.; Nielsen, A.-S.B.; Bassa, C.G.; Berthereau, A.; Bonetti, M.; Bortolas, E.; Brook, P.R.; Burgay, M.; Caballero, R.N.; et al. The second data release from the European Pulsar Timing Array—I. The dataset and timing analysis. *Astron. Astrophys.* **2023**, *678*, A48. [CrossRef]
91. Antoniadis, J.; Arumugam, P.; Arumugam, S.; Babak, S.; Bagchi, M.; Nielsen, A.-S.B.; Bassa, C.G.; Bathula, A.; Berthereau, A.; Bonetti, M.; et al. The second data release from the European Pulsar Timing Array—III. Search for gravitational wave signals. *Astron. Astrophys.* **2023**, *678*, A50. [CrossRef]
92. Xu, H.; Chen, S.; Guo, Y.; Jiang, J.; Wang, B.; Xu, J.; Xue, Z.; Caballero, R.N.; Yuan, J.; Xu, Y.; et al. Searching for the Nano-Hertz Stochastic Gravitational Wave Background with the Chinese Pulsar Timing Array Data Release I. *Res. Astron. Astrophys.* **2023**, *23*, 075024. [CrossRef]
93. Agazie, G.; Anumarlapudi, A.; Archibald, A.M.; Baker, P.T.; Bécsy, B.; Blecha, L.; Bonilla, A.; Brazier, A.; Brook, P.R.; Burke-Spolaor, S.; et al. The NANOGrav 15 yr Data Set: Constraints on Supermassive Black Hole Binaries from the Gravitational-wave Background. *Astrophys. J. Lett.* **2023**, *952*, L37. [CrossRef]
94. Afzal, A.; Agazie, G.; Anumarlapudi, A.; Archibald, A.M.; Arzoumanian, Z.; Baker, P.T.; Bécsy, B.; Blanco-Pillado, J.J.; Blecha, L.; Boddy, K.K.; et al. The NANOGrav 15 yr Data Set: Search for Signals from New Physics. *Astrophys. J. Lett.* **2023**, *951*, L11. [CrossRef]
95. Antoniadis, J.; Arumugam, P.; Arumugam, S.; Auclair, P.; Babak, S.; Bagchi, M.; Nielsen, A.-S.B.; Barausse, E.; Bassa, C.G.; Bathula, A.; et al. The second data release from the European Pulsar Timing Array: IV. Implications for massive black holes, dark matter and the early Universe. *arXiv* **2023**, arXiv:2306.16227.
96. Ellis, J.; Fairbairn, M.; Hütsi, G.; Raidal, J.; Urrutia, J.; Vaskonen, V.; Veermäe, H. Gravitational waves from supermassive black hole binaries in light of the NANOGrav 15-year data. *Phys. Rev. D* **2024**, *109*, L021302. [CrossRef]
97. Shen, Z.Q.; Yuan, G.W.; Wang, Y.Y.; Wang, Y.Z. Dark Matter Spike surrounding Supermassive Black Holes Binary and the nanohertz Stochastic Gravitational Wave Background. *arXiv* **2023**, arXiv:2306.17143.
98. Bi, Y.C.; Wu, Y.M.; Chen, Z.C.; Huang, Q.G. Implications for the supermassive black hole binaries from the NANOGrav 15-year data set. *Sci. China Phys. Mech. Astron.* **2023**, *66*, 120402. [CrossRef]
99. Barausse, E.; Dey, K.; Crisostomi, M.; Panayada, A.; Marsat, S.; Basak, S. Implications of the pulsar timing array detections for massive black hole mergers in the LISA band. *Phys. Rev. D* **2023**, *108*, 103034. [CrossRef]
100. Addazi, A.; Cai, Y.F.; Marciano, A.; Visinelli, L. Have pulsar timing array methods detected a cosmological phase transition? *Phys. Rev. D* **2024**, *109*, 015028. [CrossRef]
101. Athron, P.; Fowlie, A.; Lu, C.T.; Morris, L.; Wu, L.; Wu, Y.; Xu, Z. Can supercooled phase transitions explain the gravitational wave background observed by pulsar timing arrays? *arXiv* **2023**, arXiv:2306.17239.
102. Zu, L.; Zhang, C.; Li, Y.Y.; Gu, Y.; Tsai, Y.L.S.; Fan, Y.Z. Mirror QCD phase transition as the origin of the nanohertz Stochastic Gravitational-Wave Background. *Sci. Bull.* **2024**, *69*, 741–746. [CrossRef] [PubMed]
103. Jiang, S.; Yang, A.; Ma, J.; Huang, F.P. Implication of nano-Hertz stochastic gravitational wave on dynamical dark matter through a dark first-order phase transition. *Class. Quant. Grav.* **2024**, *41*, 065009. [CrossRef]
104. Xiao, Y.; Yang, J.M.; Zhang, Y. Implications of nano-Hertz gravitational waves on electroweak phase transition in the singlet dark matter model. *Sci. Bull.* **2023**, *68*, 3158–3164. [CrossRef] [PubMed]
105. Abe, K.T.; Tada, Y. Translating nano-Hertz gravitational wave background into primordial perturbations taking account of the cosmological QCD phase transition. *Phys. Rev. D* **2023**, *108*, L101304. [CrossRef]
106. Gouttenoire, Y. First-Order Phase Transition Interpretation of Pulsar Timing Array Signal Is Consistent with Solar-Mass Black Holes. *Phys. Rev. Lett.* **2023**, *131*, 171404. [CrossRef] [PubMed]
107. An, H.; Su, B.; Tai, H.; Wang, L.T.; Yang, C. Phase transition during inflation and the gravitational wave signal at pulsar timing arrays. *arXiv* **2023**, arXiv:2308.00070.
108. Kitajima, N.; Nakayama, K. Nanohertz gravitational waves from cosmic strings and dark photon dark matter. *Phys. Lett. B* **2023**, *846*, 138213. [CrossRef]
109. Ellis, J.; Lewicki, M.; Lin, C.; Vaskonen, V. Cosmic superstrings revisited in light of NANOGrav 15-year data. *Phys. Rev. D* **2023**, *108*, 103511. [CrossRef]
110. Wang, Z.; Lei, L.; Jiao, H.; Feng, L.; Fan, Y.Z. The nanohertz stochastic gravitational wave background from cosmic string loops and the abundant high redshift massive galaxies. *Sci. China Phys. Mech. Astron.* **2023**, *66*, 120403. [CrossRef]

111. Antusch, S.; Hinze, K.; Saad, S.; Steiner, J. Singling out SO(10) GUT models using recent PTA results. *Phys. Rev. D* **2023**, *108*, 095053. [CrossRef]
112. Ahmed, W.; Chowdhury, T.A.; Nasri, S.; Saad, S. Gravitational waves from metastable cosmic strings in the Pati-Salam model in light of new pulsar timing array data. *Phys. Rev. D* **2024**, *109*, 015008. [CrossRef]
113. Ahmed, W.; Rehman, M.U.; Zubair, U. Probing stochastic gravitational wave background from SU(5) $\times$ U(1) strings in light of NANOGrav 15-year data. *J. Cosmol. Astropart. Phys.* **2024**, *01*, 049. [CrossRef]
114. Basilakos, S.; Nanopoulos, D.V.; Papanikolaou, T.; Saridakis, E.N.; Tzerefos, C. Gravitational wave signatures of no-scale supergravity in NANOGrav and beyond. *Phys. Lett. B* **2024**, *850*, 138507. [CrossRef]
115. Chen, Z.C.; Huang, Q.G.; Liu, C.; Liu, L.; Liu, X.J.; Wu, Y.; Wu, Y.M.; Yi, Z.; You, Z.Q. Prospects for Taiji to detect a gravitational-wave background from cosmic strings. *J. Cosmol. Astropart. Phys.* **2024**, *03*, 022. [CrossRef]
116. Kitajima, N.; Lee, J.; Murai, K.; Takahashi, F.; Yin, W. Gravitational waves from domain wall collapse, and application to nanohertz signals with QCD-coupled axions. *Phys. Lett. B* **2024**, *851*, 138586. [CrossRef]
117. Blasi, S.; Mariotti, A.; Rase, A.; Sevrin, A. Axionic domain walls at Pulsar Timing Arrays: QCD bias and particle friction. *J. High Energy Phys.* **2023**, *11*, 169. [CrossRef]
118. Babichev, E.; Gorbunov, D.; Ramazanov, S.; Samanta, R.; Vikman, A. NANOGrav spectral index γ=3 from melting domain walls. *Phys. Rev. D* **2023**, *108*, 123529. [CrossRef]
119. Franciolini, G.; Iovino, A.J.; Vaskonen, V.; Veermae, H. Recent Gravitational Wave Observation by Pulsar Timing Arrays and Primordial Black Holes: The Importance of Non-Gaussianities. *Phys. Rev. Lett.* **2023**, *131*, 201401. [CrossRef] [PubMed]
120. Liu, L.; Chen, Z.C.; Huang, Q.G. Implications for the non-Gaussianity of curvature perturbation from pulsar timing arrays. *Phys. Rev. D* **2024**, *109*, L061301. [CrossRef]
121. Vagnozzi, S. Inflationary interpretation of the stochastic gravitational wave background signal detected by pulsar timing array experiments. *J. High Energy Astrophys.* **2023**, *39*, 81–98. [CrossRef]
122. Cai, Y.F.; He, X.C.; Ma, X.H.; Yan, S.F.; Yuan, G.W. Limits on scalar-induced gravitational waves from the stochastic background by pulsar timing array observations. *Sci. Bull.* **2023**, *68*, 2929–2935. [CrossRef]
123. Wang, S.; Zhao, Z.C.; Li, J.P.; Zhu, Q.H. Implications of pulsar timing array data for scalar-induced gravitational waves and primordial black holes: Primordial non-Gaussianity fNL considered. *Phys. Rev. Res.* **2024**, *6*, L012060. [CrossRef]
124. Jin, J.H.; Chen, Z.C.; Yi, Z.; You, Z.Q.; Liu, L.; Wu, Y. Confronting sound speed resonance with pulsar timing arrays. *J. Cosmol. Astropart. Phys.* **2023**, *09*, 016. [CrossRef]
125. You, Z.Q.; Yi, Z.; Wu, Y. Constraints on primordial curvature power spectrum with pulsar timing arrays. *J. Cosmol. Astropart. Phys.* **2023**, *11*, 065. [CrossRef]
126. Yi, Z.; You, Z.Q.; Wu, Y.; Chen, Z.C.; Liu, L. Exploring the NANOGrav Signal and Planet-mass Primordial Black Holes through Higgs Inflation. *arXiv* **2023**, arXiv:2308.14688.
127. Yi, Z.; You, Z.Q.; Wu, Y. Model-independent reconstruction of the primordial curvature power spectrum from PTA data. *J. Cosmol. Astropart. Phys.* **2024**, *01*, 066. [CrossRef]
128. Bringmann, T.; Depta, P.F.; Konstandin, T.; Schmidt-Hoberg, K.; Tasillo, C. Does NANOGrav observe a dark sector phase transition? *J. Cosmol. Astropart. Phys.* **2023**, *11*, 053. [CrossRef]
129. Zhang, Z.; Cai, C.; Su, Y.H.; Wang, S.; Yu, Z.H.; Zhang, H.H. Nano-Hertz gravitational waves from collapsing domain walls associated with freeze-in dark matter in light of pulsar timing array observations. *Phys. Rev. D* **2023**, *108*, 095037. [CrossRef]
130. Yi, Z.; Gao, Q.; Gong, Y.; Wang, Y.; Zhang, F. Scalar induced gravitational waves in light of Pulsar Timing Array data. *Sci. China Phys. Mech. Astron.* **2023**, *66*, 120404. [CrossRef]
131. Chen, Z.C.; Li, J.; Liu, L.; Yi, Z. Probing the speed of scalar-induced gravitational waves with pulsar timing arrays. *Phys. Rev. D* **2024**, *109*, L101302. [CrossRef]
132. Zhu, X.J.; Cui, W.; Thrane, E. The minimum and maximum gravitational-wave background from supermassive binary black holes. *Mon. Not. Roy. Astron. Soc.* **2019**, *482*, 2588–2596. [CrossRef]
133. Li, J.; Chen, Z.C.; Huang, Q.G. Measuring the tilt of primordial gravitational-wave power spectrum from observations. *Sci. China Phys. Mech. Astron.* **2019**, *62*, 110421; Erratum in *Sci. China Phys. Mech. Astron.* **2021**, *64*, 250451. [CrossRef]
134. Chen, Z.C.; Yuan, C.; Huang, Q.G. Non-tensorial gravitational wave background in NANOGrav 12.5-year data set. *Sci. China Phys. Mech. Astron.* **2021**, *64*, 120412. [CrossRef]
135. Wu, Y.M.; Chen, Z.C.; Huang, Q.G. Constraining the Polarization of Gravitational Waves with the Parkes Pulsar Timing Array Second Data Release. *Astrophys. J.* **2022**, *925*, 37. [CrossRef]
136. Chen, Z.C.; Wu, Y.M.; Huang, Q.G. Searching for isotropic stochastic gravitational-wave background in the international pulsar timing array second data release. *Commun. Theor. Phys.* **2022**, *74*, 105402. [CrossRef]
137. Chen, Z.C.; Wu, Y.M.; Huang, Q.G. Search for the Gravitational-wave Background from Cosmic Strings with the Parkes Pulsar Timing Array Second Data Release. *Astrophys. J.* **2022**, *936*, 20. [CrossRef]
138. Wu, Y.M.; Chen, Z.C.; Huang, Q.G.; Zhu, X.; Bhat, N.D.R.; Feng, Y.; Hobbs, G.; Manchester, R.N.; Russell, C.J.; Shannon, R.M. Constraining ultralight vector dark matter with the Parkes Pulsar Timing Array second data release. *Phys. Rev. D* **2022**, *106*, L081101. [CrossRef]

139. Falxa, M.; Babak, S.; Baker, P.T.; Bécsy, B.; Chalumeau, A.; Chen, S.; Chen, Z.; Cornish, N.J.; Guillemot, L.; Hazboun, J.S.; et al. Searching for continuous Gravitational Waves in the second data release of the International Pulsar Timing Array. *Mon. Not. Roy. Astron. Soc.* **2023**, *521*, 5077–5086. [CrossRef]
140. Wu, Y.M.; Chen, Z.C.; Huang, Q.G. Search for stochastic gravitational-wave background from massive gravity in the NANOGrav 12.5-year dataset. *Phys. Rev. D* **2023**, *107*, 042003. [CrossRef]
141. Wu, Y.M.; Chen, Z.C.; Huang, Q.G. Pulsar timing residual induced by ultralight tensor dark matter. *J. Cosmol. Astropart. Phys.* **2023**, *09*, 021. [CrossRef]
142. Agazie, G.; Antoniadis, J.; Anumarlapudi, A.; Archibald, A.M.; Arumugam, P.; Arumugam, S.; Arzoumanian, Z.; Askew, J.; Babak, S.; Bagchi, M.; et al. Comparing Recent Pulsar Timing Array Results on the Nanohertz Stochastic Gravitational-wave Background. *Astrophys. J.* **2024**, *966*, 105. [CrossRef]
143. Malik, K.A.; Wands, D. Cosmological perturbations. *Phys. Rep.* **2009**, *475*, 1–51. [CrossRef]
144. Inomata, K.; Kawasaki, M.; Mukaida, K.; Tada, Y.; Yanagida, T.T. Inflationary primordial black holes for the LIGO gravitational wave events and pulsar timing array experiments. *Phys. Rev. D* **2017**, *95*, 123510. [CrossRef]
145. Espinosa, J.R.; Racco, D.; Riotto, A. A Cosmological Signature of the SM Higgs Instability: Gravitational Waves. *J. Cosmol. Astropart. Phys.* **2018**, *09*, 012. [CrossRef]
146. Ashton, G.; Huebner, M.; Lasky, P.D.; Talbot, C.; Ackley, K.; Biscoveanu, S.; Chu, Q.; Divarkala, A.; Easter, P.J.; Goncharov, B.; et al. BILBY: A user-friendly Bayesian inference library for gravitational-wave astronomy. *Astrophys. J. Suppl.* **2019**, *241*, 27. [CrossRef]
147. Skilling, J. Nested Sampling. *AIP Conf. Proc.* **2004**, *735*, 395–405. [CrossRef]
148. Moore, C.J.; Vecchio, A. Ultra-low-frequency gravitational waves from cosmological and astrophysical processes. *Nat. Astron.* **2021**, *5*, 1268–1274. [CrossRef]